Hints for universality in coupled map lattices

Frederick H. Willeboordse*
Department of Physics, The National University of Singapore, Singapore 119260
(Received 14 June 2001; revised manuscript received 21 September 2001; published 3 January 2002)

A wide range of coupled map lattices is found to have identical pattern sequences providing numerical evidence for their universality in the class of systems studied. It is furthermore found that the wave-type solutions of the diffusively coupled logistic lattice scale linearly with the coupling range indicating the existence of a continuum limit. The findings are used to introduce a very simple type of spatially extended map that can serve as a representative for the pattern sequence of this class of coupled maps.

DOI: 10.1103/PhysRevE.65.026202 PACS number(s): 05.45.Ra

I. INTRODUCTION

Coupled map lattices have widely been studied as paradigms for high dimensional chaos due to their rich phenomenology and computational efficiency. Especially the nearest neighbor diffusively and the globally coupled logistic lattices have been investigated numerically in great detail (for a general introduction, see e.g., [1,2] or [3–5] for nearest neighbor coupled logistic maps and [6–8] for globally coupled logistic maps).

Intermediate regimes or the dependency of the phenomenologies on the forms of the couplings and local maps have thus far received little attention. Recently, however, a combination of a local map with a global map has yielded some interesting results [9], while the origin of power-law correlations for nonlocal couplings was theoretically explained in [10] for medium range nonlocal couplings. In this paper, the effects of extending the coupling range and the sensitivity of the phenomenology on the local map and the coupling form are investigated.

Two main discoveries and a very simple coupled map are reported. First, it is found that when extending the coupling range in the diffusively coupled logistic lattice, the attractor (a wave-type solution) scales linearly with the coupling range. This provides numerical evidence of a proper continuum limit. Second, it is found that the phenomenology of the diffusively coupled logistic lattice is applicable to a wide variety of coupled maps. The latter finding is used to introduce a tent-map-like coupled map that is extremely simple and that does not have a local chaotic map. This coupled map can serve as a representative for the investigated class of coupled maps as with regards to the pattern sequence.

II. LONG RANGE COUPLINGS AND THE CONTINUUM LIMIT

Adding the coupling range as a variable, the standard diffusively coupled logistic lattice can be extended as

$$x_{n+1}^i=(1-\varepsilon)f(x_n^i)+\frac{\varepsilon}{2r}\sum_{k=1}^{r}[f(x_n^{i-k})+f(x_n^{i+k})], \quad (1)$$

where $f(x)$ is the single logistic map

$$f(x_n)=x_{n+1}=1-\alpha x_n^2 \quad (2)$$

with α the nonlinearity, ε the coupling constant, and r the coupling range.

For $r=1$, when increasing the nonlinearity in Eq. (1) from 0 to the maximum 2, the system encounters several so-called universality classes such as e.g., patterns with kinks, frozen random patterns, pattern selection, and traveling waves. Not surprisingly, the phenomenology for globally coupled maps is rather different with, for example, the formation of hierarchical clusters, marginal stability with information avalanches [11] or high dimensional tori [8,12,13]. For larger values of the coupling constant ε and medium high values of the nonlinearity α, the globally coupled map has a single uniform solution while the nearest neighbor coupled map has a temporally period four wavelike solution.

It is found that for $r>1$ in Eq. (1), the shape and temporal periodicity of the attractor remain unchanged while the wavelength increases. An example of a long wavelength solution in shown in Fig. 1 where the selected pattern for $r=20$ is depicted.

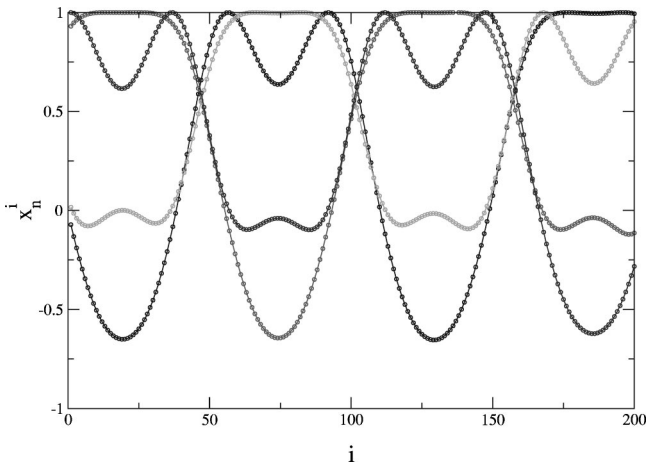

FIG. 1. Attractor with a wavelength of 114 sites and a coupling range of 20. Only the first 200 sites of a lattice of 1145 sites are shown. The system size was chosen to be ten times the wavelength as determined in Fig. 3 in order to minimize frustration. The nonlinearity $\alpha=1.7$ and the coupling constant $\varepsilon=0.7$.

*Email address: willeboordse@yahoo.com URL: http://staff.science.nus.edu.sg/~frederik

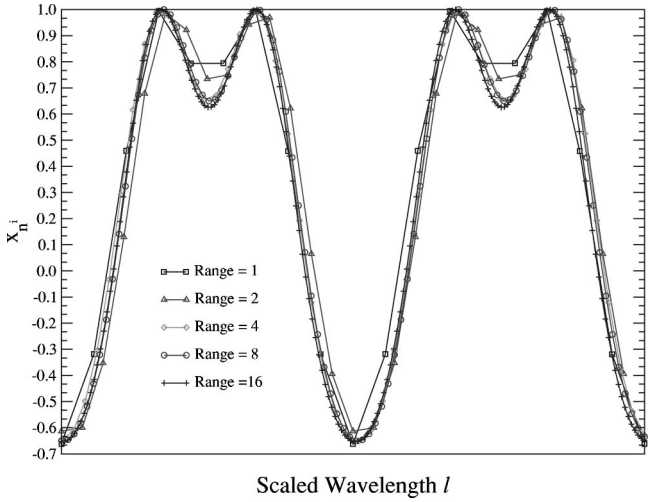

FIG. 2. Scaled overlay of five attractors with coupling ranges from $r=1$ to $r=16$ as indicated in the figure. The nonlinearity $\alpha=1.7$ and the coupling constant $\varepsilon=0.7$.

In order to examine how well the solution scales, attractors with increasing coupling ranges were compared by scaling and shifting the x axis such that the start and end points of a single pulse of the same phase match. As can be seen in Fig. 2, the overlap of successively longer waves becomes better for increasing r. Indeed, when plotting the wavelength versus the coupling range as in Fig. 3, it is found that the scaling is linear to a very high accuracy. The data were obtained by calculating the average wavelength of 100 runs with a transient time of 50 000 steps for each value of r. In order to minimize the effects of frustration, the system size N was increased for increasing coupling ranges by setting it to $N=600r$ assuring that for each coupling range r, there is a sufficient number of pulses for determining the wavelength.

The data provide clear numerical evidence for a continuum limit. This may be of great physical interest, especially if a corresponding partial differential equation can be found. Phenomenologically, Eq. (1) turns out to basically behave equivalently for all r when taking the effects of frustration into account. This does not mean, however, that there cannot be any differences. In the case of the frozen random pattern (and the pattern with kinks), for example, the initial conditions must roughly be chosen in segments of size r in order to obtain the frozen random attractor. This is as expected since the segments of the frozen random pattern are determined by the domain size of neighboring lattice points in the same band of the single logistic map [14].

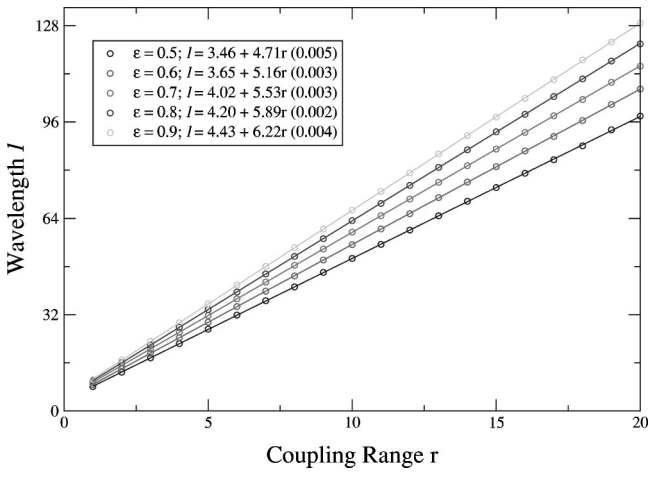

FIG. 3. Wavelength versus the coupling range for the coupled map in Eq. (1). The nonlinearity $\alpha=1.7$ and the coupling constant ε ranges from 0.5 to 0.9 as indicated. The small circles represent actual data points while the lines are the result of linear regression with the indicated correlation coefficient.

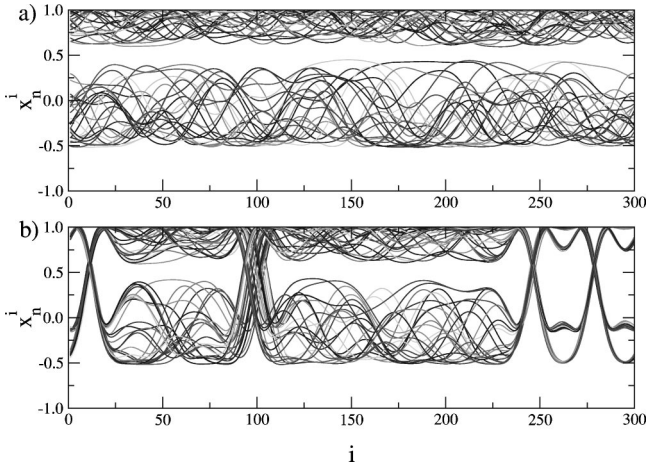

FIG. 4. Different attractors depending on the range of the initial conditions. In (a) the initial conditions are chosen randomly for each site between -1 and 1. In (b) r neighboring sites have an identical random value between -1 and 1. The parameters are $\alpha=1.52$, $\varepsilon=0.7$, and $r=10$ with the system size $N=300$.

The difference between random initial conditions and segmented random initial conditions is illustrated in Fig. 4 where typical patterns for both cases are depicted (naturally since the values are random, the two cases are not mutually exclusive). As can be seen, for completely random initial conditions, the system falls on what appears to be a supertransient chaotic band 2 attractor as found in the nearest neighbor diffusively coupled logistic lattice [14–16], while for the segmented initial conditions the expected (scaled) frozen random pattern is obtained.

In order to verify whether the band 2 attractor is indeed a supertransient, first the transient times for a range of small system sizes were determined by averaging 10 000 runs (see the inset in the upper left corner of Fig. 5) to find the one-pulse system size with the least amount of frustration. Next the transient times for four to seven times this system size were determined by averaging over 100 runs. The motivation for this procedure is that otherwise, in order to exclude major artifacts due to frustration, system sizes would need to be chosen that would lead to impractically long transient times. As can be seen in Fig. 5, the transient time indeed increases exponentially indicating the supertransient nature of the attractor.

In the limit where the coupling range approaches the system size (i.e., $r\rightarrow N$), Eq. (1) becomes more and more similar to the globally coupled map. It is well-known that for larger values of ε, the globally coupled map is attracted to a

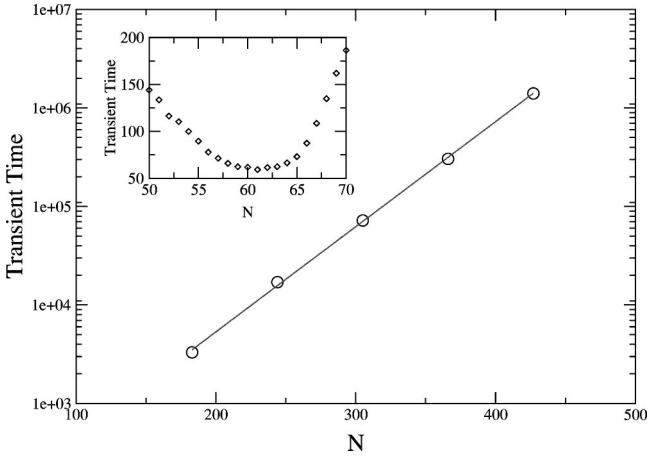

FIG. 5. Transient time versus system size for the two band attractors shown in Fig. 4. The parameters are $\alpha=1.52$, $\varepsilon=0.7$, and $r=10$ and the system size ranges from $N=183$ to $N=427$. The inset in the left upper corner shows the average transient time versus the system size for small system sizes big enough for just one pulse. The shortest transient time (and hence the best fit) is for $N=61$.

uniform state. In light of the current findings, this can be understood by considering that a wave-type solution at least needs one pulse. When the system size becomes too small to squeeze in a pulse with frustration, only a part of the pulse remains. Due to the equalizing effects of the coupling, this part will then be flattened to the homogeneous attractor if the overall curvature of the segment is small enough. Indeed, it is found that for system size independent wavelengths l, as determined by extrapolating Fig. 3, up to $l\approx\frac{3}{2}N$ periodic solutions exist, possibly with remnant or superimposed chaos. For $\frac{3}{2}N\approx l\approx 2N$, spatially smooth but nonhomogeneous sine-pulse-segment-like, temporally chaotic, solutions exist, while for $l\approx 2N$, the spatially homogeneous, temporally chaotic, attractor equivalent to the single logistic map as found in the globally coupled map is selected.

For smaller values of ε and not too short coupling ranges

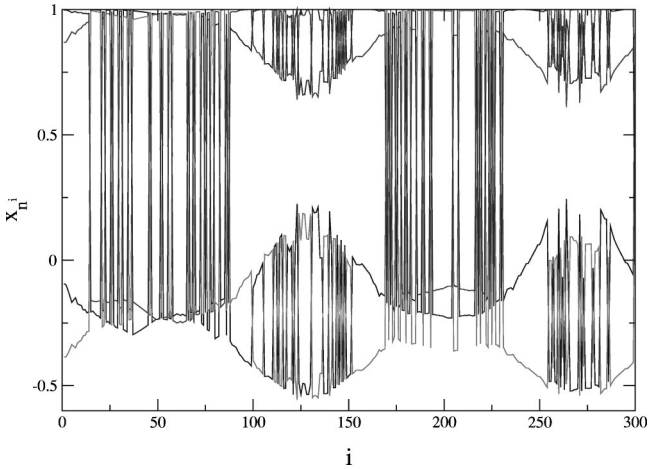

FIG. 6. Superposition of globally coupled maplike solutions and long coupling range wavelike solutions. The parameters are $\alpha=1.7$, $\varepsilon=0.22$, and $r=50$.

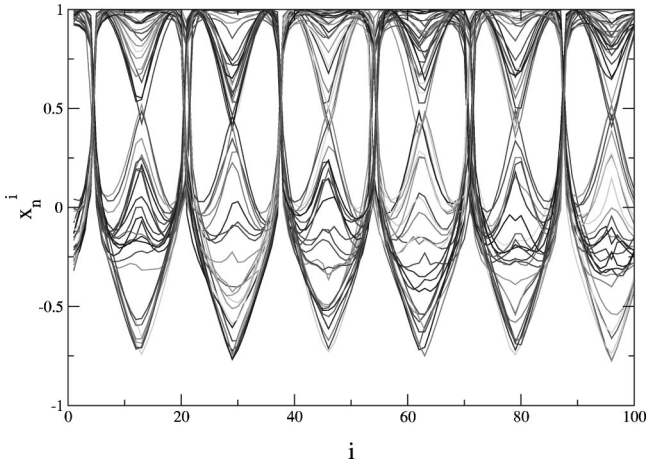

FIG. 7. Chaotic pattern selection of type 1. The parameters are $\alpha=1.8$, $\varepsilon=0.4$, and $r=8$.

r, mixed or superposed states can be found as can be seen in Fig. 6.

III. CHAOTIC PATTERN SELECTION

Besides the mixed or superposed states, two types of chaotic pattern selection (CPS) not found in a similar way in either the very short range or very long range regimes are shown in Figs. 7 and 8. Both types display a long range order combined with local chaos.

In the first type, depicted in Fig. 7, overall at each time step, the attractor is very similar to the pattern selection attractor. While the nodes are fixed in space, however, the segments in between appear to chaotically approximate one of the phases of the attractor. Visually, CPS is somewhat reminiscent of frustration induced chaotic motion on a selected pattern. If frustration would be the source of the observed chaos, a clear dependence on the system size should be observed. This was not found to be the case, however, when simulating the system repeatedly for several hundred million time steps with lattice sizes around $N=1000$ and a coupling range of $r=8$ yielding a wavelength of about 33.

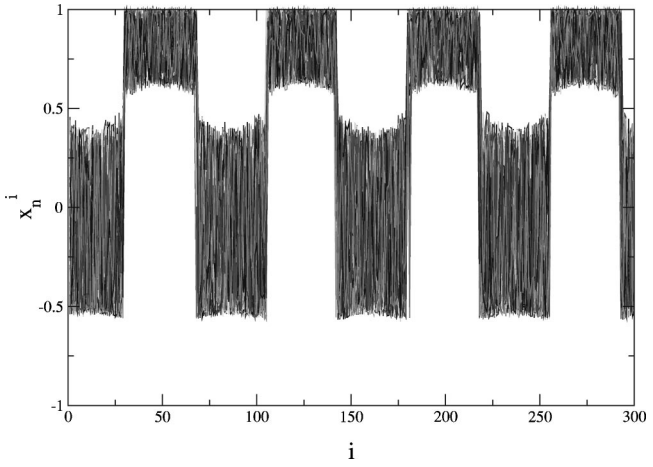

FIG. 8. Chaotic pattern selection of type 2. The parameters are $\alpha=1.7$, $\varepsilon=0.065$, and $r=50$.

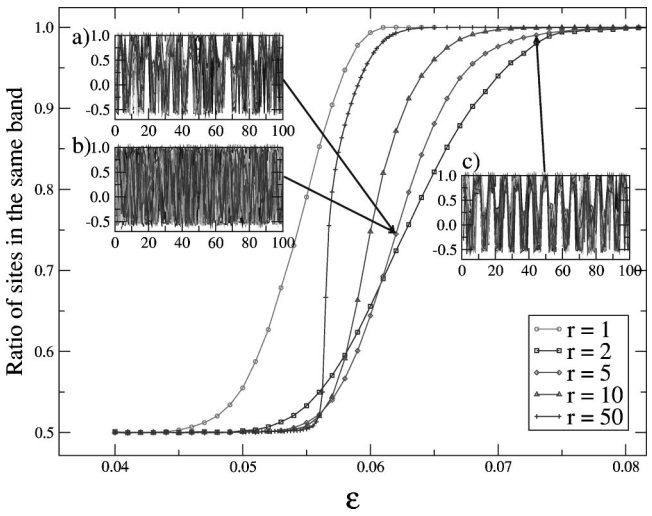

FIG. 9. The ratio of sites that, when starting in either the lower or upper band, is found to be in the same band 100 iterates later. The average over 10^6 time steps is taken after a transient of 10^5 time steps. The system sizes are $N=100$ for $r=1$, $N=200$ for $r=2,5,10$, and $N=300$ for $r=50$. The nonlinearity is $\alpha=1.7$. The insets show some representative space-amplitude plots. In (a) every second iterate is plotted and in (b) every 100th iterate is plotted for $r=5$ and $\varepsilon=0.62$. In (c) every 100th iterate is plotted for $r=5$ and $\varepsilon=0.73$.

This ratio of wavelength to system size should be sufficiently small to exclude frustration as the source for this type of CPS.

The second type of chaotic pattern selection, depicted in Fig. 8, occurs in a narrow band for values of ε slightly larger than those that yield the spatiotemporal chaos found for small ε. The transition from spatiotemporal chaos to chaotic pattern selection appears to be smooth (at least as long as r is not too big) as can be seen in Fig. 9 where the ratio of lattice sites that are found in the same band at one time step and 100 iterates later is plotted versus ε (the patterns are temporally period 2). While this ratio includes sites that flip back and forth, after the transients have mostly died out, it provides a good indication of the temporal stability of the pattern.

When increasing ε from the spatiotemporal region, the temporal stability of the pattern slowly increases, i.e., the time sites remain in the same band increases gradually. At first sites remain in the same band only for very short times. Then they do so for longer times disturbed by frequent defects. As in the type 2 intermittency found in the nearest neighbor diffusively coupled logistic lattice, these defects can spontaneously arise. Lastly, when the ratio is just reaching one, regularly spaced chaotic pattern selection can be found. This is illustrated in the insets of Fig. 9. In (a) and (b), the parameters are identical but the time scales are different. In (a), where the spatiotemporal pattern can clearly be discerned, every second iterate is plotted revealing the short-time dynamics, while in (b), resembling spatiotemporal chaos, every 100th iterate is plotted. Inset (c) shows chaotic pattern selection (some defects remain for these parameters) for a value of ε at which the ratio of sites found in the same band is nearly 1.

With the exception of $r=1$, the curves become steeper and move to the left for increasing coupling strengths. For $r=1$, when increasing the coupling strength beyond the range where chaotic pattern selection is found, an inverse bifurcation sequence to the spatially and temporally period 2 zigzag pattern occurs. This was not found for $r>1$, where the lattice seems to freeze nonperiodically, possibly forming patterns that somewhat fall between globally coupled and locally coupled maps, before forming selected patterns for larger ε.

IV. HINTS FOR UNIVERSALITY

Since their introduction, a key motivation for the study of coupled map lattices has been the prospect of universality. In order to investigate how universal the phenomenology of the coupled logistic lattice is, the following models were simulated:

$$x_{n+1}^i=1-\frac{\alpha}{2}(x_n^{i-1}+x_n^{i+1})x_n^i \quad \text{with max}\ (x_{n+1}^i)=1, \tag{3}$$

$$x_{n+1}^i=1-\frac{\alpha}{2}\left|(x_n^{i-1}+x_n^{i+1})(x_n^i)^2\right|, \tag{4}$$

$$x_{n+1}^i=1-\frac{\alpha}{2}\left|(x_n^{i-1}+x_n^{i+1})(x_n^i)^3\right|, \tag{5}$$

$$x_{n+1}^i=1-\frac{\alpha}{3}\left|(x_n^{i-1}+x_n^{i+1})x_n^i+x_n^{i-1}x_n^{i+1}\right|, \tag{6}$$

$$x_{n+1}^i=(1-\epsilon)x_n^i+\epsilon[1-|(x_n^{i-1}+x_n^{i+1})x_n^i|]. \tag{7}$$

Equations (3)–(7), all turned out to have similar dynamics as can be seen in Fig. 10.

For comparison, Fig. 4(f) depicts pattern selection as it occurs in Eq. (1) with $r=1$.

Similar dynamics were not only observed for different types of couplings but also for local maps with higher powers in Eq. (1) ($r=1$) as is shown in Fig. 11. In order to be able to compare the phenomenology, the nonlinearity α was chosen such that the local map is just before the period-3 window except for (a) where it was chosen to be at about one-third the distance between the band merging point and maximum nonlinearity.

Figures 10 and 11 clearly show that the pattern dynamics as such is neither dependent on the exact from of the employed coupling nor dependent on the power of the local map. Indeed, it is not even dependent on having a local map at all.

A rough phenomenological phase diagram, applicable to all the lattices studied in this paper, is given in Fig. 12. In the case of the models without an explicit coupling constant [Eqs. (3)–(7)], the basic pattern sequence as depicted can be observed when increasing the nonlinearity [in Eq. (7) ε plays the role of the nonlinearity]. If the model contains a coupling constant, its increase will lead to longer wavelengths. Furthermore, in all the models investigated, increasing the cou-

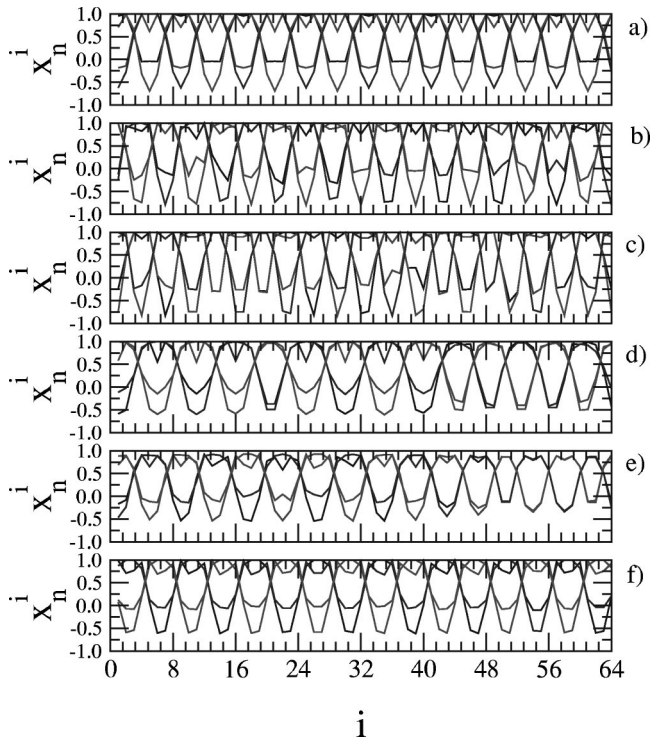

FIG. 10. Pattern selection for Eqs. (3)–(7). (a) Equation (3), $\alpha=1.7$. (b) Equation (4), $\alpha=1.81$. (c) Equation (5), $\alpha=1.84$. (d) Equation (6), $\alpha=1.65$. (e) Equation (7), $\varepsilon=0.93$. (f) Equation (1), $\alpha=1.7$, $\varepsilon=0.5$.

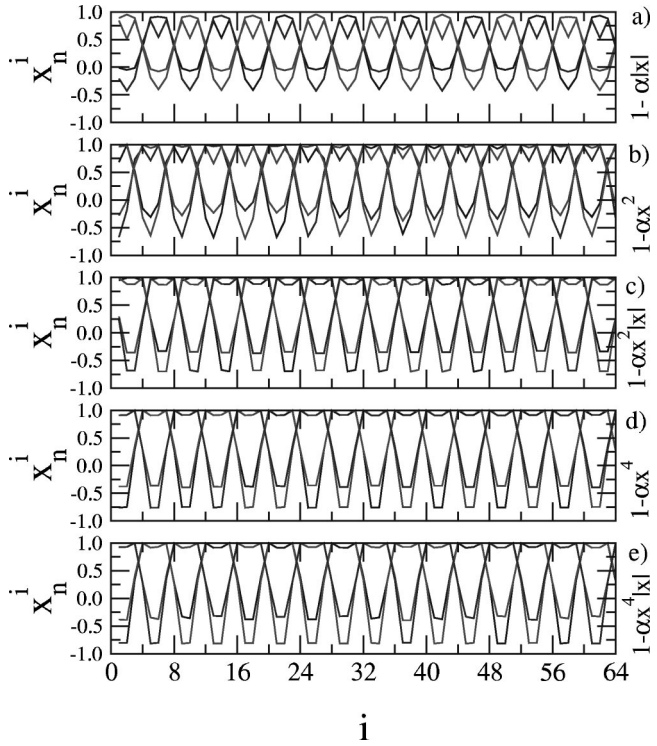

FIG. 11. Selected patterns for various local maps as indicated on the right hand side of the graphs. (a) $f(x)=1-\alpha|x|$, $\alpha=1.55$, $\varepsilon=0.5$. (b) $f(x)=1-\alpha x^2$, $\alpha=1.74$, $\varepsilon=0.6$. (c) $f(x)=1-\alpha x^2|x|$, $\alpha=1.79$, $\varepsilon=0.6$. (d) $f(x)=1-\alpha x^4$, $\alpha=1.80$, $\varepsilon=0.55$. (e) $f(x)=1-\alpha x^4|x|$, $\alpha=1.83$, $\varepsilon=0.5$.

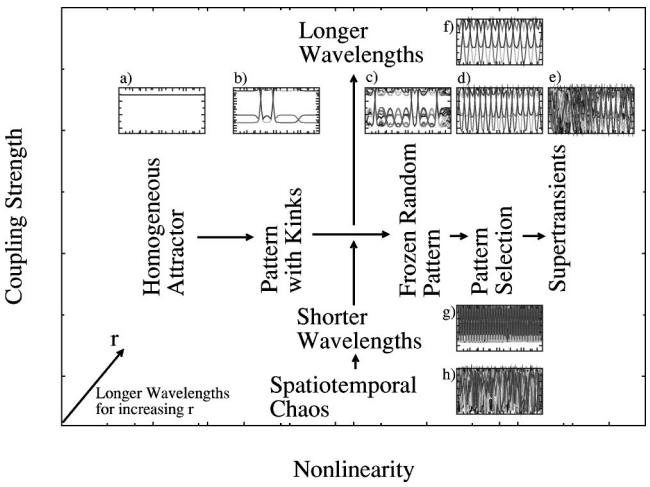

FIG. 12. Phenomenological phase diagram for the lattices studied in this paper. The insets show representative patterns from the nearest neighbor diffusively coupled logistic lattice. (a) $\alpha=0.50$, $\varepsilon=0.5$. (b) $\alpha=1.30$, $\varepsilon=0.5$. (c) $\alpha=1.45$, $\varepsilon=0.5$. (d) $\alpha=1.70$, $\varepsilon=0.5$. (e) $\alpha=1.80$, $\varepsilon=0.5$. (f) $\alpha=1.70$, $\varepsilon=0.8$. (g) $\alpha=1.70$, $\varepsilon=0.085$. (h) $\alpha=1.70$, $\varepsilon=0.04$.

pling range r resulted in an increase of the wavelength and in an increase of the similarity between the wave shapes. The numerical results, therefore, strongly hint at the existence of an underlying universal mechanism.

V. THE TENT-COUPLING MAP AS A SIMPLE PARADIGM

In order to provide a simple paradigm for the pattern sequence observed in Eq. (1) and Eqs. (3)–(7), the following tent-coupling map was studied

$$x_{n+1}^i=1-\frac{\alpha}{2}|(x_n^{i-1}+x_n^{i+1})x_n^i|, \tag{8}$$

where i is the spatial index, n the discrete time, and α a parameter. Just as in the case of the diffusively coupled map, Eq. (8) can straightforwardly be extended to longer coupling ranges

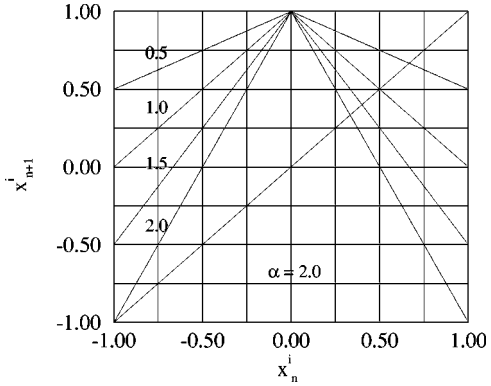

FIG. 13. The tent-coupling map of Eq. (8) for several given values of $x_n^{i-1}+x_n^{i+1}$ as indicated in the figure for $\alpha=2.0$.

$$x_{n+1}^{i}=1-\frac{\alpha}{2r}\left|\sum_{k=1}^{r}(x_n^{i-k}+x_n^{i+k})x_n^{i}\right|. \tag{9}$$

As immediately can be seen, in the homogeneous case, Eq. (8) reduces to the single logistic map, while for a given state of the neighbors it forms the tent map given in Fig. 13 where the slope is determined by the product of the nonlinearity α and the sum of the neighbors.

As with the other models used in this paper, it is found that the pattern sequence observed for Eq. (8) goes from a uniform state to (supertransient) spatiotemporal chaos via patterns with kinks, frozen random patterns, and pattern selection. Even traveling waves have been observed for $\alpha=1.75$ and $r=2$.

VI. CONCLUSION

In conclusion, it was found that a variety of coupled maps displays identical pattern sequences when increasing the nonlinearity. It was furthermore found that the patterns scale when increasing the coupling range. In the case of the diffusively coupled logistic lattice, the scaling is linear providing clear numerical evidence for a continuum limit. The two findings combined provide thus far the strongest evidence yet of the existence of universality classes in coupled map lattices. The very simple introduced tent-coupling map appears to be suitable as a paradigm for the pattern sequence in this class of coupled maps.

ACKNOWLEDGMENT

I am grateful to Kunihiko Kaneko for stimulating feedback and valuable suggestions on the manuscript.

[1] J. P. Crutchfield and K. Kaneko, *Directions in Chaos* (World Scientific, Singapore, 1987).
[2] K. Kaneko, *Theory and Applications of Coupled Map Lattices* (Wiley, New York, 1993).
[3] K. Kaneko, Physica D **34**, 1 (1989).
[4] F. H. Willeboordse, Chaos, Solitons Fractals **2**, 609 (1992).
[5] F. H. Willeboordse and K. Kaneko, Phys. Rev. Lett. **73**, 533 (1994).
[6] K. Kaneko, Phys. Rev. Lett. **69**, 905 (1992).
[7] K. Kaneko, Physica D **86**, 158 (1995).
[8] K. Kaneko, Physica D **54**, 5 (1991).
[9] N. B. Ouchi and K. Kaneko, Chaos **10**, 359 (2000).
[10] Y. Kuramoto and H. Nakao, Phys. Rev. Lett. **76**, 4352 (1996).
[11] K. Kaneko, Physica D **77**, 456 (1994).
[12] K. Wiesenfeld and P. Hadley, Phys. Rev. Lett. **62**, 1335 (1989).
[13] S. H. Strogatz and R. E. Mirollo, Phys. Rev. E **47**, 220 (1993).
[14] F. H. Willeboordse, Phys. Lett. A **183**, 187 (1993).
[15] K. Kaneko, Phys. Lett. A **149**, 105 (1990).
[16] F. H. Willeboordse, Chaos **4**, 89 (1994).